Solar Radiative Transfer in Cirrus Clouds. Part II: Theory and Computation of Multiple Scattering in an Anisotropic Medium

YOSHIHIDE TAKANO AND KUO-NAN LIOU

Department of Meteorology, University of Utah, Salt Lake City, Utah

(Manuscript received 1 February 1988, in final form 13 June 1988)

ABSTRACT

We have developed a theoretical framework for the computation of the transfer of solar radiation in an anisotropic medium with particular application to oriented ice crystals in cirrus clouds. In the theoretical development, the adding principle for radiative transfer has been used with modifications to account for the anisotropy of the phase matrix. The single-scattering properties, including the phase function, single-scattering albedo, and extinction cross section, for randomly and horizontally oriented ice crystals are then used in the computation of reflected and transmitted intensities, planetary albedo, and polarization in multiple scattering. There are significant differences in the reflected and transmitted intensities between hexagonal ice crystals and equivalent ice spheres. In addition, it is found that ice spheres are inadequate to model the general pattern of reflected intensity. The orientation properties of ice crystals are also significant in the determination of the reflected and transmitted intensities. Various optical features can be produced only by horizontally oriented plates and columns. For the polarization of sunlight reflected by ice crystals, the neutral point is independent of the solar zenith angle as well as the optical depth. We have also closely matched the polarization patterns observed for Martian white clouds, as well as cirrus clouds, with the results from the present multiple-scattering computations for ice crystals. Finally, it is noted that the polarization configuration is extremely sensitive to the shape of the particles. Thus, its full information content should be explored for applications to the remote sounding of clouds.

1. Introduction

The interpretation of bidirectional reflectance and polarization patterns for planetary clouds observed from aircraft, satellites, or spacecraft requires multiple-scattering calculations for cloud particles. Multiple scattering in clouds is also important for the determination of cloud albedo, which is relevant to climate problems. There have been numerous methods developed for solving multiple scattering in planetary atmospheres. The adding method has been demonstrated to be a powerful tool for multiple-scattering calculations. The principle for the method was stated by Stokes (1862) in a problem dealing with reflection and transmission by glass plates. Peebles and Plesset (1951) developed the adding method theory for application to gamma-ray transfer. The adding equations for multiple scattering now commonly used are based on the formulation presented by van de Hulst in 1963 (van de Hulst 1980). We shall use the adding method for the formulation of multiple scattering in an anisotropic medium.

As pointed out in Part I (Takano and Liou 1988, hereafter referred to as Part I), cirrus clouds are composed of hexagonal ice crystals, whose single-scattering properties differ significantly from those computed for spherical particles. Moreover, in the case of horizontally oriented ice crystals, the single-scattering parameters depend on the direction of the incident light beam. Thus, the conventional formulation for the multiple-scattering problem is no longer applicable. Liou (1980) formulated the basic equation for the transfer of solar radiation in an optically anisotropic medium in which the single-scattering properties vary with the incident angle of the light beam. Stephens (1980) and Asano (1983) discussed the transfer of radiation through optically anisotropic ice clouds. The latter author used a hypothetical cloud model in which the scattering phase function was expressed in terms of the incident angle. However, none of these authors included realistic scattering parameters for oriented ice crystals in the discussion and analysis, nor is the Stokes vector properly accounted for in the formulation.

This paper presents the theory and computations for multiple scattering in cirrus clouds containing oriented ice crystals. In section 2, radiative transfer in clouds composed of horizontally oriented ice crystals is formulated with the aid of the adding method. Using the single-scattering properties obtained in Part I, the reflected and transmitted intensities, planetary albedo, and polarization in multiple scattering by ice crystals are illustrated and discussed in section 3. In section 4,

Corresponding author address: Dr. Kuo-Nan Liou, Dept. of Meteorology, 819 Wm. C. Browning Building, University of Utah, Salt Lake City, UT 84112.

we interpret a number of polarization measurements based on computational results from randomly oriented ice crystals. Finally, conclusions are given in section 5.

2. Theory of radiative transfer in an anisotropic medium

In an anisotropic medium, the single-scattering properties depend on the direction of the incoming light beam. Let the directions of incoming and outgoing light beams be denoted by (μ', ϕ') and (μ, ϕ), respectively, where μ is the cosine of the zenith angle and ϕ the corresponding azimuthal angle. The scattering phase matrix $\mathbf{P}$ is a function of $(\mu, \phi; \mu', \phi')$ and cannot be defined by the scattering angle Θ alone as in conventional radiative transfer. Moreover, the extinction (σ_e or C_e in Part I) and scattering (σ_s or C_s in Part I) cross sections vary with the direction of the incoming light beam (μ', ϕ').

Consider an anisotropic medium consisting of ice crystals randomly oriented in a horizontal plane. Because of the symmetry with respect to the azimuthal angle for the incoming light beam, the phase matrix, and the extinction and scattering cross sections may be expressed by $\mathbf{P}(\mu, \phi; \mu', \phi')$ $[=\mathbf{P}(\Theta, \Phi, \mu')]$, $\sigma_e(\mu')$, and $\sigma_s(\mu')$, respectively, where Φ is the azimuthal angle associated with the scattering angle Θ. In this case, we may define the differential normal optical depth in the form

$$\frac{d\tilde{\tau}}{dz} = -\tilde{\sigma}_e N_0, \tag{1}$$

where the normal extinction cross section $\tilde{\sigma}_e = \sigma_e(\mu' = 1)$, N_0 is the number density of the particles, and z the distance. Let the Stokes vector intensity $\mathbf{I} = (I, Q, U, V)$. Following Liou (1980), the general equation governing the transfer of diffuse solar intensity may be written in the form

$$\mu \frac{d\mathbf{I}(\tilde{\tau}; \mu, \phi)}{d\tau} = \mathbf{I}(\tilde{\tau}; \mu, \phi)k(\mu) - \vec{\mathbf{J}}(\tilde{\tau}; \mu, \phi), \tag{2}$$

where

$$k(\mu) = \sigma_e(\mu)/\tilde{\sigma}_e, \tag{3}$$

and the source function,

$$\vec{\mathbf{J}}(\tilde{\tau}; \mu, \phi) = \frac{1}{4\pi}\int_0^{2\pi}\int_{-1}^{1} \tilde{\omega}(\mu')\mathbf{P}(\mu, \phi; \mu', \phi') \times \mathbf{I}(\tilde{\tau}; \mu', \phi')d\mu' d\phi' + \frac{1}{4\pi}\tilde{\omega}(-\mu_0)\mathbf{P}(\mu, \phi; -\mu_0, \phi_0) \times \pi\vec{\mathbf{F}}_0 \exp[-k(-\mu_0)\tilde{\tau}/\mu_0]. \tag{4}$$

In Eq. (4), μ_0 is the cosine of the solar zenith angle, ϕ_0 the corresponding azimuthal angle, and $-\mu_0$ denotes the downward solar incident direction. The first and second terms on the right-hand side represent contributions from multiple scattering and single scattering of the direct solar intensity, respectively. The equivalent single-scattering albedo is defined by

$$\tilde{\omega}(\mu) = \sigma_s(\mu)/\tilde{\sigma}_e. \tag{5}$$

The general phase matrix, with respect to the local meridian plane, is given by (Chandrasekhar 1960; Liou 1980)

$$\mathbf{P}(\mu, \mu'; \phi - \phi') = \mathbf{L}(\pi - i_2)\mathbf{P}(\Theta, \Phi, \mu')\mathbf{L}(-i_1), \tag{6}$$

where i_1 and i_2 denote the angles between the meridian planes for the incoming and outgoing light beams, respectively, and the plane of scattering. The transformation matrix for the Stokes vector is given by

$$\mathbf{L}(\chi) = \begin{bmatrix} 1 & 0 & 0 & 0 \\ 0 & \cos 2\chi & \sin 2\chi & 0 \\ 0 & -\sin 2\chi & \cos 2\chi & 0 \\ 0 & 0 & 0 & 1 \end{bmatrix}, \tag{7}$$

where $\chi = -i_1$ or $\pi - i_2$. From spherical geometry, these angles are given by

$$\cos i_1 = \frac{-\mu + \mu' \cos\Theta}{\pm(1 - \cos^2\Theta)^{1/2}(1 - \mu'^2)^{1/2}}, \tag{8}$$

$$\cos i_2 = \frac{-\mu' + \mu \cos\Theta}{\pm(1 - \cos^2\Theta)^{1/2}(1 - \mu^2)^{1/2}}. \tag{9}$$

If $P(\Theta, \Phi, \mu)$, $\sigma_e(\mu)$, and $\sigma_s(\mu)$ are known, then, in principle, Eq. (2) may be solved numerically.

We shall approach the multiple scattering problem by means of the adding method for radiative transfer. We define the reflection matrix $\mathbf{R}(\mu, \mu_0, \phi - \phi_0)$ and transmission matrix $\mathbf{T}(\mu, \mu_0; \phi - \phi_0)$ for radiation from above in the forms

$$\mathbf{I}_{\text{out, top}}(\mu, \phi) = \frac{1}{\pi}\int_0^1 \mu_0 d\mu_0 \int_0^{2\pi} d\phi_0 \times \mathbf{R}(\mu, \mu_0; \phi - \phi_0)\mathbf{I}_{\text{in, top}}(\mu_0, \phi_0), \tag{10}$$

$$\mathbf{I}_{\text{out, bottom}}(\mu, \phi) = \frac{1}{\pi}\int_0^1 \mu_0 d\mu_0 \int_0^{2\pi} d\phi_0 \times \mathbf{T}(\mu, \mu_0; \phi - \phi_0)\mathbf{I}_{\text{in, top}}(\mu_0, \phi_0). \tag{11}$$

Likewise, for radiation from below, the reflection and transmission matrices are defined by

$$\mathbf{I}_{\text{out, bottom}}(\mu, \phi) = \frac{1}{\pi}\int_0^1 \mu_0 d\mu_0 \int_0^{2\pi} d\phi_0 \times \mathbf{R}^*(\mu, \mu_0; \phi - \phi_0)\mathbf{I}_{\text{in, bottom}}(\mu_0, \phi_0), \tag{12}$$

$$\mathbf{I}_{\text{out, top}}(\mu, \phi) = \frac{1}{\pi}\int_0^1 \mu_0 d\mu_0 \int_0^{2\pi} d\phi_0 \times \mathbf{T}^*(\mu, \mu_0; \phi - \phi_0)\mathbf{I}_{\text{in, bottom}}(\mu_0, \phi_0). \tag{13}$$

To proceed with the adding principle for radiative transfer in an anisotropic medium, we shall utilize the reflection and transmission matrices defined in Eqs. (10)–(13) and consider an infinitesimal layer with a very small optical depth $\Delta\tilde{\tau}$, say 10^{-8}. Since the optical

depth is so small, only single scattering takes place within the layer. From Eqs. (2) and (4), the analytic solutions for reflected and transmitted intensities undergoing single scattering may be derived. Subject to the condition that $\Delta\tilde{\tau} \to 0$, we find

$$\mathbf{T}(\mu, \mu_0; \phi - \phi_0) \approx \frac{\Delta\tilde{\tau}}{4\mu\mu_0} \tilde{\omega}(\mu_0)\mathbf{P}(\mu, \mu_0; \phi - \phi_0), \tag{14}$$

$$\mathbf{R}(\mu, \mu_0; \phi - \phi_0) \approx \frac{\Delta\tilde{\tau}}{4\mu\mu_0} \tilde{\omega}(\mu_0)\mathbf{P}(-\mu, \mu_0; \phi - \phi_0), \tag{15}$$

$$\mathbf{T}^*(\mu, \mu_0; \phi - \phi_0) \approx \frac{\Delta\tilde{\tau}}{4\mu\mu_0} \tilde{\omega}(\mu_0)\mathbf{P}(-\mu, -\mu_0; \phi - \phi_0), \tag{16}$$

$$\mathbf{R}^*(\mu, \mu_0; \phi - \phi_0) \approx \frac{\Delta\tilde{\tau}}{4\mu\mu_0} \tilde{\omega}(\mu_0)\mathbf{P}(\mu, -\mu_0; \phi - \phi_0), \tag{17}$$

where the phase matrix $\mathbf{P}$ is defined in Eq. (6).

Consider now two layers, one on top of the other. Let the subscripts a and b denote these two layers and let their optical depths be $\tilde{\tau}_a$ and $\tilde{\tau}_b$. Following the conventional adding principle for radiative transfer in an isotropic medium (see, e.g., Twomey et al. 1966; Lacis and Hansen 1974; Liou 1980), but with modifications to account for the dependence of the optical properties on the incoming direction, the procedure for computing the reflection and transmission matrices for the composite layer may be described by the following equations:

$$\mathbf{Q}_1 = \mathbf{R}_a^*\mathbf{R}_b, \tag{18}$$

$$\mathbf{Q}_n = \mathbf{Q}_1\mathbf{Q}_{n-1}, \tag{19}$$

$$\mathbf{S} = \sum_{n=1}^{M} \mathbf{Q}_n, \tag{20}$$

$$\mathbf{D} = \mathbf{T}_a + \mathbf{S}\exp[-k(\mu_0)\tilde{\tau}_a/\mu_0] + \mathbf{S}\mathbf{T}_a, \tag{21}$$

$$\mathbf{U} = \mathbf{R}_b\exp[-k(\mu_0)\tilde{\tau}_a/\mu_0] + \mathbf{R}_b\mathbf{D}, \tag{22}$$

$$\mathbf{R}_{a,b} = \mathbf{R}_a + \exp[-k(\mu)\tilde{\tau}_a/\mu]\mathbf{U} + \mathbf{T}_a^*\mathbf{U}, \tag{23}$$

$$\mathbf{T}_{a,b} = \exp[-k(\mu)\tilde{\tau}_b/\mu]\mathbf{D} + \mathbf{T}_b\exp[-k(\mu_0)\tilde{\tau}_a/\mu_0] + \mathbf{T}_b\mathbf{D}. \tag{24}$$

In these equations, the product of two functions implies an integration over the appropriate solid angle so that all possible multiple scattering contributions are accounted for. For example,

$$\mathbf{R}_a^*\mathbf{R}_b = \frac{1}{\pi}\int_0^{2\pi}\int_0^1 \mathbf{R}_a^*(\mu, \mu'; \phi - \phi') \times \mathbf{R}_b(\mu', \mu_0; \phi' - \phi_0)\mu' d\mu' d\phi'. \tag{25}$$

The term M in Eq. (20) is selected according to the convergence of the series, and varies from 5 to 12 in the present calculations. The exponential terms in the adding equations are the direct transmission through layer a or b without scattering, where the anisotropic factor $k(\mu)$ is given in Eq. (3). The total transmission for the combined layer is the sum of the diffuse transmission $\mathbf{T}_{a,b}$ and the direct transmission $\exp[-k(\mu_0)(\tilde{\tau}_a + \tilde{\tau}_b)/\mu_0]$ in the direction of the solar zenith angle θ_0.

In the numerical computations, it is economical to set $\tilde{\tau}_a = \tilde{\tau}_b$. This is referred to as the doubling method. We start with an optical depth $\tilde{\tau} \approx 10^{-8}$ and use Eqs. (14)–(17) to compute the reflection and transmission matrices. Equations (18)–(24) are subsequently employed to compute the reflection and transmission matrices for an optical depth of $2\tilde{\tau}$. The computations using these equations are repeated until the desired optical depth is obtained.

In order to compute the reflection and transmission matrices for the initial layer with a very small optical depth, via Eqs. (14)–(15), we need the phase matrix and single-scattering albedo, and directions for incoming and outgoing beams. The phase matrix elements must be expanded in terms of the incoming and outgoing directions denoted by μ, μ' and $\phi - \phi'$. For spherical particles, the phase matrix consists of four nonzero independent elements. These elements can be decoupled analytically in terms of functions associated with μ, μ' and $\phi - \phi'$ (Dave 1970; Kattawar et al. 1973). However, for nonspherical particles, the decomposition of the phase matrix elements has yet to be worked out. For randomly oriented nonspherical particles that have a plane of symmetry, the phase matrix contains six independent elements. In this case, there are seven symmetrical relationships for these elements based on the reciprocity principle (Hovenier 1969). From these relationships, the phase matrix elements can be expanded in terms of either cosine or sine Fourier components (Hansen 1971). For randomly oriented ice plates or columns in a horizontal plane, there are 16 elements in the phase matrix. It can be proven that these elements obey a number of symmetrical relationships, upon which they can be expanded in terms of either cosine or sine Fourier components in the manner described by Hansen (1971).

In view of the above discussion, the general phase matrix elements may be numerically expanded in the forms

$$\tilde{\omega}(\mu')P_{ij}(\mu, \mu'; \phi - \phi') = P_{ij}^0(\mu, \mu') + 2\sum_{m=1}^{N} p_{ij}^m(\mu, \mu')\begin{cases}\cos m(\phi - \phi'), & c \\ \sin m(\phi - \phi'), & s\end{cases} \tag{26}$$

where

$$c, ij = 11, 12, 21, 22, 33, 34, 43, 44$$

$$s, ij = 13, 14, 23, 24, 31, 32, 41, 42$$

and P_{ij}^m ($m = 0, 1, \cdots, N$) denote the Fourier expansion coefficients. With this expansion, each term in the Fourier series may be treated independently in numerical computations.

With respect to the normalization of the phase function P_{11}, the following procedures are followed. The phase function is normalized such that

$$\frac{1}{4\pi}\int_0^{2\pi}\int_{-1}^{1} P_{11}(\mu, \mu', \phi - \phi')d\mu d(\phi - \phi') = 1, \quad (27a)$$

where $d\mu d(\phi - \phi')$ denotes the differential solid angle. Using Eq. (26), we find

$$\frac{1}{2}\int_{-1}^{1} P_{11}^0(\mu, \mu')d\mu = \tilde{\omega}(\mu'), \quad (27b)$$

where $\tilde{\omega}(\mu')$ is defined in Eq. (5). In the case of randomly oriented nonspherical particles (or spherical particles), the single-scattering albedo $\tilde{\omega}$ is independent of μ' and is a constant. If there is no absorption, $\tilde{\omega} = 1$. In this case, Eq. (27b) can be derived from the expansion of the phase function in terms of the Legendre polynomial using the addition theorem for spherical harmonics (see, e.g., Liou 1980). However, for randomly oriented ice crystals in a horizontal plane, $\tilde{\omega}$ is a function of the incident angle. Normalization of the phase function must be performed for each μ'.

As shown in Part I, the phase function P_{11} for ice crystals has a common sharp diffraction peak. In order to properly account for this peak in numerical integrations, thousands of Fourier components are needed in the phase function expansion. To optimize the computational effort, we shall follow the procedure proposed by Potter (1970). In this procedure, the forward peak is truncated by extrapolating the phase function linearly from the scattering angles 10° to 0° in the logarithmic scale. Let the truncated phase function be P_{11}^t; then, the truncated fraction of scattered intensity is given by

$$f = \int_{4\pi} (P_{11} - P_{11}^t)d\Omega/4\pi. \quad (28)$$

In our numerical computations, we find that $f \approx f_D$, the ratio of the diffracted light to the entire scattered light, described in the appendix of Part I. In the limits of geometric ray optics, it is apparent that the scattered energy contained in the truncated forward peak, which is the shaded area in Fig. A1 of Part I, is approximately equal to the scattered energy associated with Fraunhoffer diffraction.

To use the truncated phase function in multiple scattering computations, but at the same time to achieve the "equivalent" result as in the case when the sharp diffraction peak was included in the computations, an adjustment must be made for the optical depth and single-scattering albedo. Since the forward peak is associated only with scattering, the adjusted scattering and absorption optical depth must be $\tilde{\tau}_s' = (1 - f)\tilde{\tau}_s$ and $\tilde{\tau}_a' = \tilde{\tau}_a$. Thus, the adjusted optical depth should be

$$\tilde{\tau}' = \tilde{\tau}_s' + \tilde{\tau}_a' = (1 - f\tilde{\omega})\tilde{\tau}, \quad (29)$$

where the single-scattering albedo $\tilde{\omega} = \tilde{\tau}_s/\tilde{\tau}$. The adjusted single-scattering albedo is

$$\tilde{\omega}' = \frac{\tilde{\tau}_s'}{\tilde{\tau}'} = \frac{(1 - f)\tilde{\omega}}{1 - f\tilde{\omega}}. \quad (30)$$

In addition to the preceding adjustment, we must also account for the contribution of the δ-transmission part f_δ, associated with the forward scattering at $\Theta = 0°$ described in the appendix of Part I, which cannot be included in numerical computations. Following the above procedure, the optical thickness $\tilde{\tau}''$ and single-scattering albedo $\tilde{\omega}''$, which are corrected for this δ-function peak, are given by

$$\tilde{\tau}'' = (1 - f_\delta\tilde{\omega}')\tilde{\tau}', \quad (31)$$

$$\tilde{\omega}'' = \frac{(1 - f_\delta)\tilde{\omega}'}{1 - f_\delta\tilde{\omega}'}. \quad (32)$$

For conservative scattering, the adjustment is required only for the optical depth. In the case of 2-D crystals, f and f_δ depend on the incident direction θ_0, as well as the extinction and scattering cross sections, σ_e and σ_s. Equations (29)–(32) constitute the generalized similarity principle for radiative transfer in horizontally oriented polyhedral particles. The similarity principle has been discussed by Sobolev (1975) for isotropic scattering and van de Hulst (1980), who included the asymmetry factor in the discussion.

3. Computational results

In this section we present computational results for reflected and transmitted intensities, planetary albedo, and reflected polarization for randomly (3-D) and horizontally (2-D) oriented ice crystals using a visible wavelength of 0.55 μm. In the computations, the number of emergent angles μ used for 2-D columns is 20. For 2-D plates, Parry columns, and 3-D columns and plates, it is 40. Azimuthal angular intervals of 1° were used. These angular intervals are adequate to produce smooth curves for the reflected and transmitted intensities.

Figure 1 shows the reflected and transmitted (diffuse) intensities for 3-D ice columns ($L/2a = 125$ μm/50 μm) and area-equivalent ice spheres as a function of the zenith angle θ for an overhead sun ($\theta_0 = 0°$). The reflected intensity increases with increasing optical depth. Significant differences between the reflected intensities for ice columns and spheres are seen. Ice spheres produce a peak intensity at $\theta = 45°$, associated with a combination of primary and secondary rainbow features due to single-scattering. But ice columns have larger reflected intensities in other zenith angle regions. In the transmitted intensity pattern, the 22° and 46°

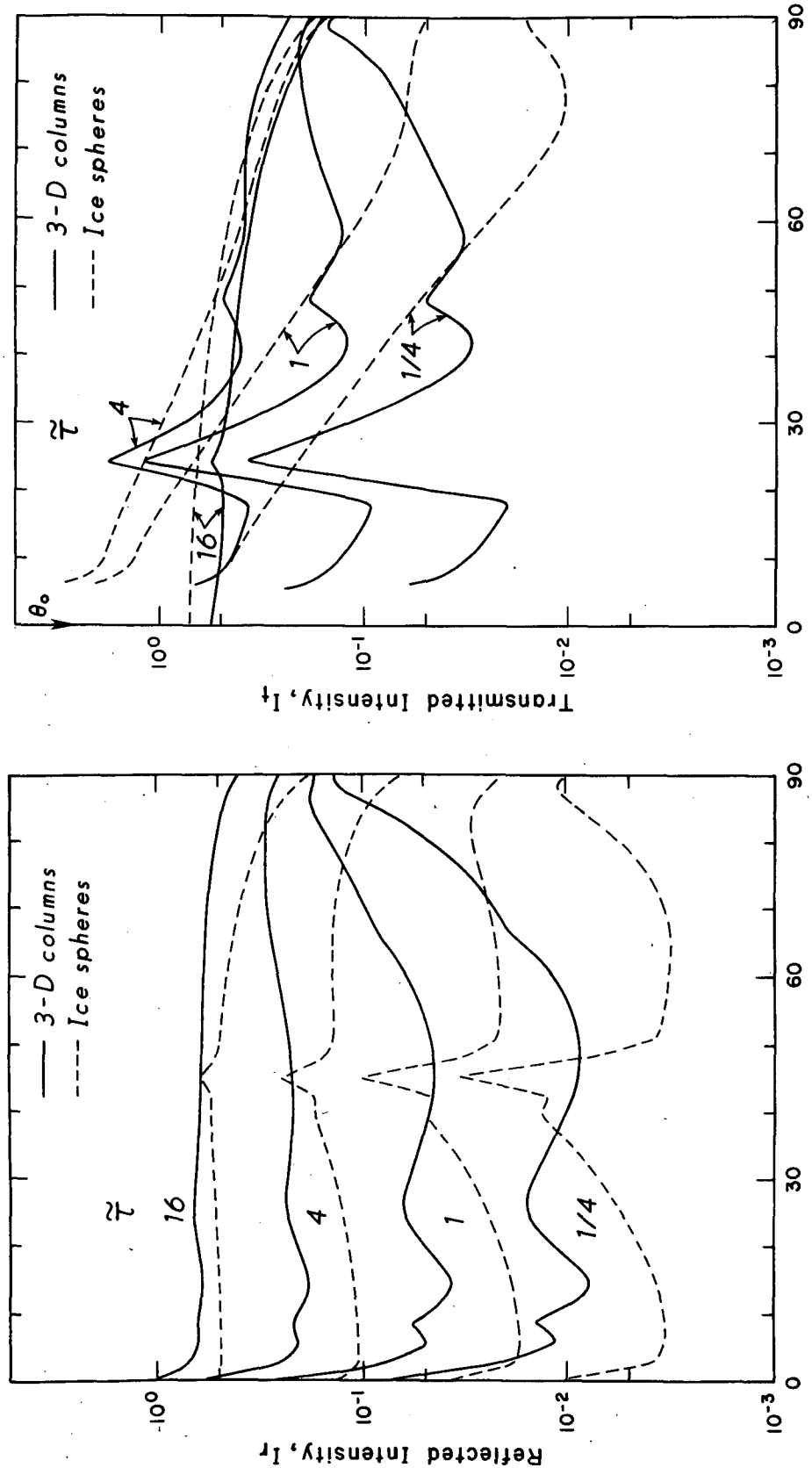

FIG. 1. Intensity reflected and transmitted by 3-D columns ($L/2a$ = 125 μm/50 μm) and area-equivalent spheres with an overhead sun ($\theta_0 = 0°$) at $\lambda = 0.55$ μm. The values of $\tilde{\tau}$ in 3-D and sphere cases denote the conventional optical depth.

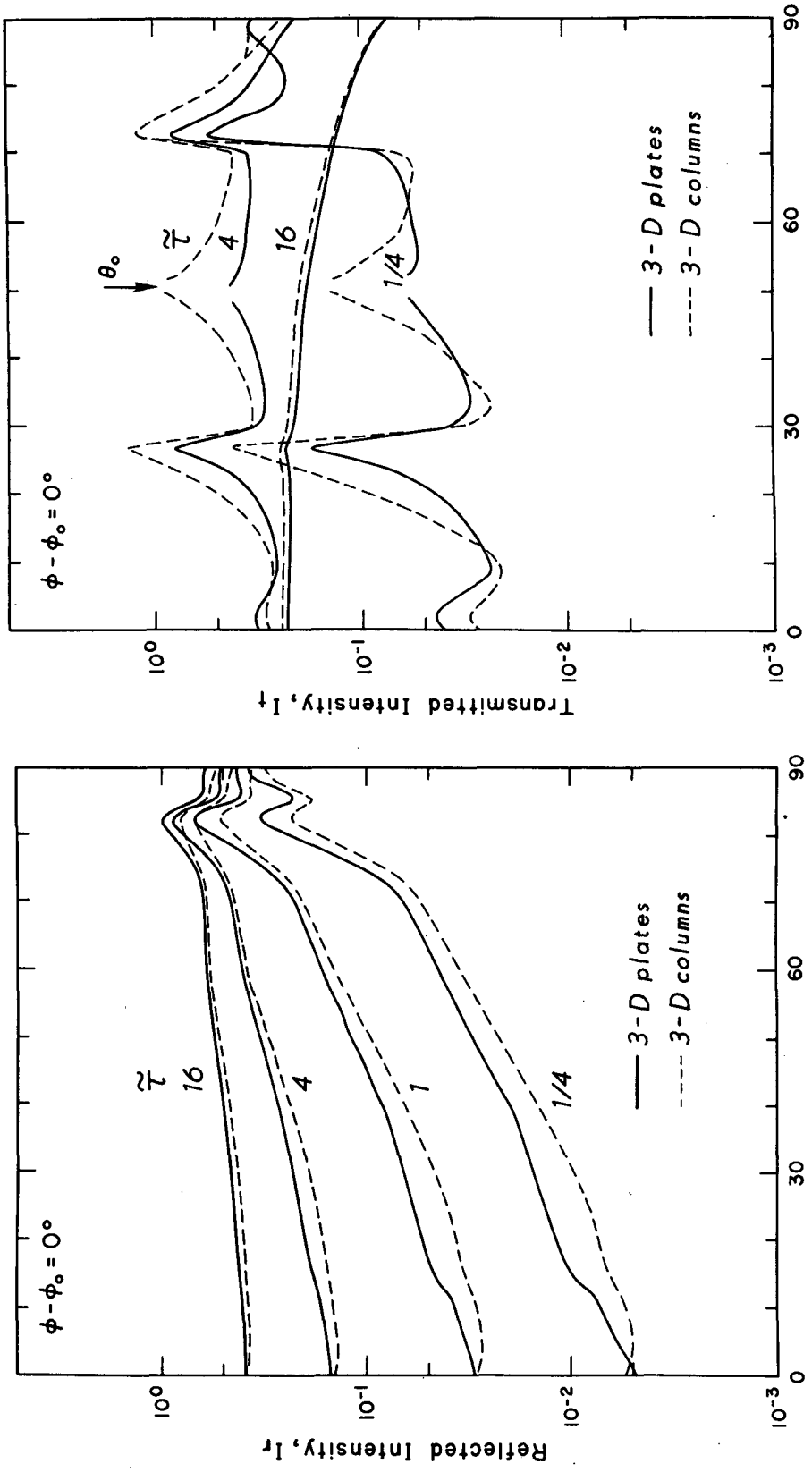

FIG. 2. Intensity reflected and transmitted by 3-D plates ($L/2a = 0.4$) and 3-D columns ($L/2a = 2.5$) in the solar principal plane ($\phi - \phi_0 = 0°$) at $\lambda = 0.55$ μm. The solar zenith angle is 50°.

halo features produced by ice columns are very distinct for small optical depths. However, they disappear when the optical depth is greater than about 16. The transmitted intensities for ice spheres are generally larger than those for ice columns for zenith angles between 0° and ~40°, but are smaller between ~60° and 90°. We have also carried out computations for 3-D ice plates using an aspect ratio of 32 μm/80 μm. Results for the reflected and transmitted intensities are extremely similar to those for 3-D ice columns, except that the 22° halo feature for optical depths less than 4 is less pronounced.

In the preceding presentation, we have used the same crystal sizes, randomly oriented in space, in multiple-scattering computations. The scattered intensities from these computations, however, should not deviate significantly from those using the observed ice crystal size distributions shown in Fig. 2 of Part I. The reasons are as follows. First, at the 0.55 μm wavelength, absorption of ice is practically negligible so that the single-scattering albedo $\tilde{\omega} \approx 1$. Second, in multiple-scattering calculations, the optical depth is fixed. It follows that the scattered intensities depend only on the phase function employed in the calculations. The phase functions for 3-D columns (125 μm/50 μm) and 3-D plates (32 μm/80 μm), which approximately represent mean sizes of the observed ice crystal size distribution, are about the same as those presented in Fig. 3 of Part I. Thus the multiple-scattering results illustrated in this section using a single size ice crystal should be substantially similar to those using an observed ice crystal size distribution. Following the preceding reasoning, the use of area- or volume-equivalent ice spheres would produce similar multiple-scattering results. In Table 3 of Part I, we listed the asymmetry factors for area-equivalent ice spheres. For the 0.55 μm wavelength, the asymmetry factors for volume-equivalent ice spheres do not deviate substantially from those values.

In Fig. 2 we compare the reflected and transmitted intensities for 3-D plates and columns for a solar zenith angle θ_0 of 50°. These intensities are plotted as a function of the zenith angle θ on the plane $\phi - \phi_0 = 0°$. For the reflected intensity, 3-D plates reflect slightly more than 3-D columns. This is because the asymmetry factor for 3-D columns is larger than that for 3-D plates. Both columns and plates show a peak at $\theta \approx 83°$, which is associated with greater intensity at the outer halo. The patterns of the transmitted intensity are similar for the two cases. However, the transmitted intensity for plates (32 μm/80 μm) is generally smaller than that for columns (125 μm/50 μm).

The planetary albedo (referred to as reflection in radiative transfer) is defined by

$$R(\mu_0) = \frac{1}{\pi}\int_0^{2\pi}\int_0^1 I_r(\mu, \mu_0; \phi - \phi_0)\mu d\mu d\phi/(\mu_0 \pi F_0), \quad (33)$$

where $\mu_0 \pi F_0$ denotes the solar flux perpendicular to the plane-parallel atmosphere. Figure 3 shows reflection of sunlight as a function of the cosine of the solar zenith angle μ_0 for randomly oriented ice columns and plates. Comparisons are also made with area-equivalent ice spheres. Reflection by 3-D crystals is generally larger than that of spheres, and the differences increase with increasing optical depth. This is because ice spheres have larger forward scattering than ice crystals.

We next present the reflected and transmitted intensity patterns for horizontally oriented ice crystals. Figure 4 illustrates these patterns for 2-D plates when the solar zenith angle θ_0 is 75°. Note that the optical depth presented in this graph is a mean value averaged over the zenith angle θ. In the case of 2-D plates, scattered sunlight is confined to four latitude belts, due to specific geometry. For $\theta_0 = 75°$, these latitude belts correspond to zenith angles of ±75° and ±27°, with negative values representing mirror images. This is described in Eq. (21) and displayed in Fig. 7a of Part I for single-scattering analyses. If the incident angle is 27°, the four latitude belts are ±27° and ±75°. Due to the symmetrical property of 2-D plates with respect to incoming light beams, all multiple-scattered light is also confined to the four latitude belts. The reflected and transmitted intensities for optical depths of ¼, 1, 4, and 16 are displayed as a function of the azimuthal angle $\phi - \phi_0$. The reflected intensity increases with increasing optical depth. For the 75° emergent zenith angle, the subsun, subsundog, 120° subparhelion, and antisolar peak optical features are shown distinctly for an optical depth of ¼, where single-scattering dominates. For an optical depth of 16, only the subsun and subparhelion are observed. For the transmitted intensity, the sundog is visible even for large cloud optical depths. In addition to these optical phenomena, the anthelion (AN) located at the 180° azimuthal angle is seen for the small optical depth of ¼, due to double scattering, viz., the coupling of the subsun and antisolar peak. For an optical depth of 16, the 44° parhelion produced by double scattering (denoted as 44°P) is also observed. At the 27° zenith angle, the Kern's arc (KA) appears for $\tau \gtrsim 1$ due to the effects of multiple scattering. This arc has been observed by Ripley and Saugier (1971) and simulated by Tränkle and Greenler (1987) using the Monte Carlo method for multiple scattering.

Figures 5 and 6 display the reflected and transmitted intensity patterns as a function of the zenith angle on the plane $\phi - \phi_0 = 0°$ for Parry and 2-D columns, respectively. The solar zenith angle used for the computation is 75°. These patterns for an optical depth of ¼ are basically similar to those from single-scattering computations displayed in Figs. 8 and 9 of Part I, except for the subpeak at $\theta = 82°$ in the transmitted intensity in Fig. 5. This peak is caused by the lower sunvex Parry arc of the subsun. For Parry columns, several optical

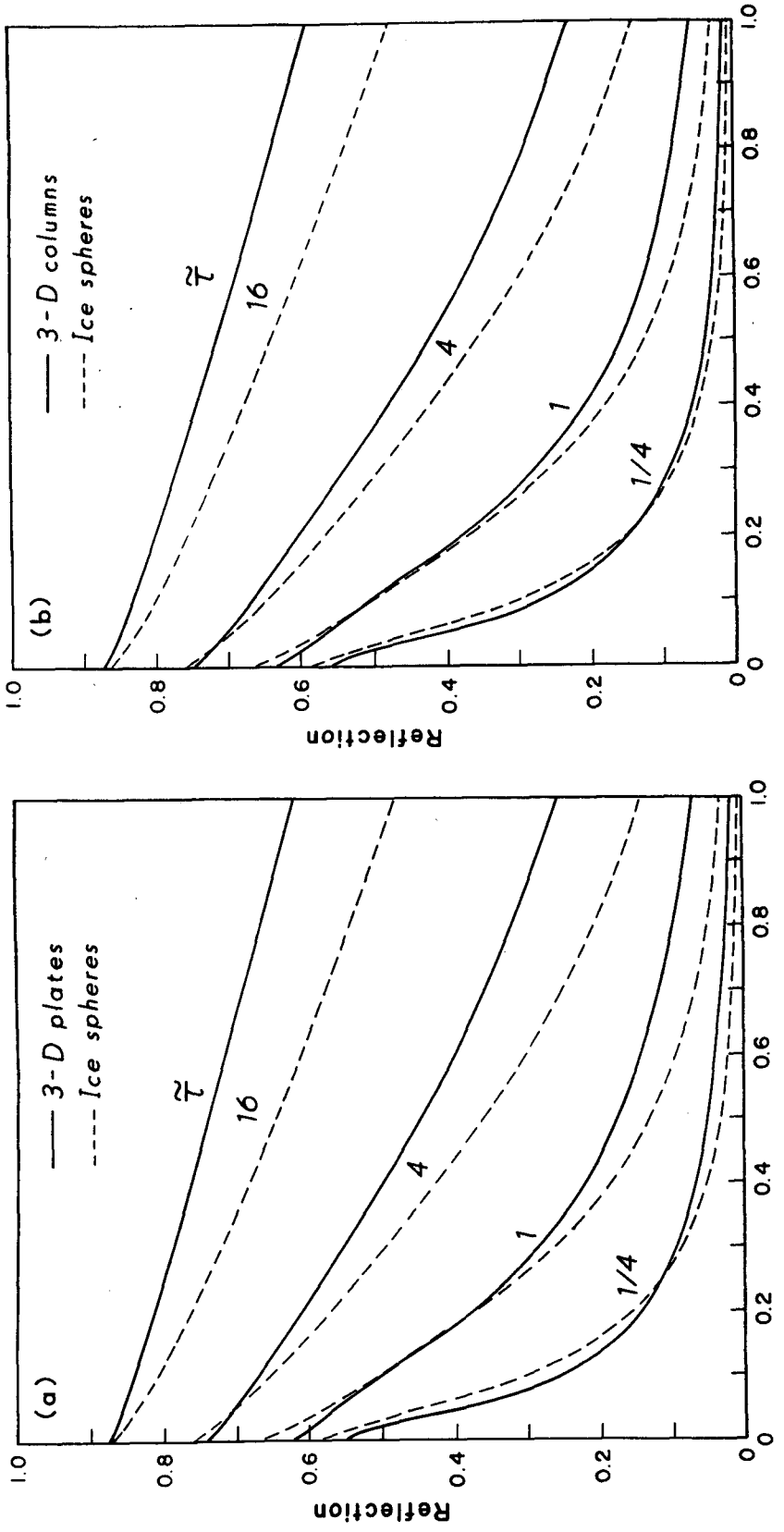

FIG. 3. Reflection for (a) 3-D plates ($L/2a$ = 32 μm/80 μm) and area-equivalent spheres as a function of the cosine of the solar zenith angle at λ = 0.55 μm, and (b) 3-D columns ($L/2a$ = 125 μm/50 μm).

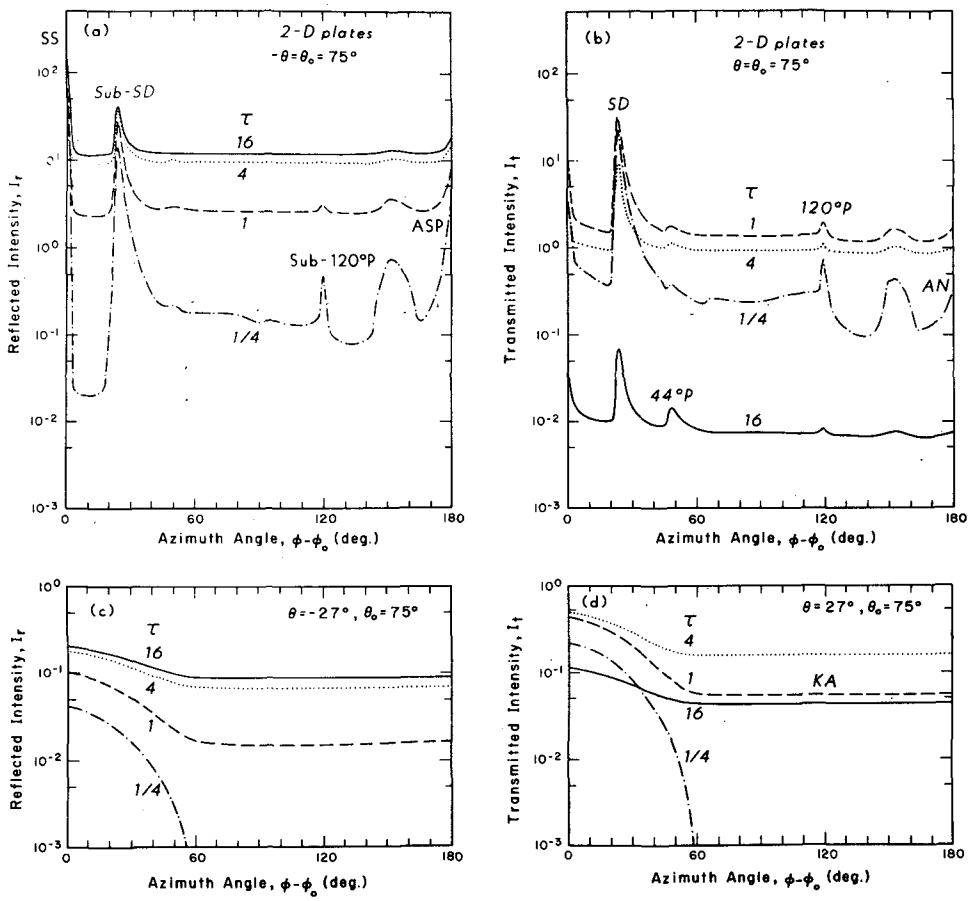

FIG. 4. Intensity of sunlight reflected and transmitted by 2-D plates ($L/2a = 0.1$) as a function of the azimuth angle, $\phi - \phi_0$ for (a) $-\theta = \theta_0 = 75°$, (b) $\theta = \theta_0 = 75°$, (c) $(\theta, \theta_0) = (-27°, 75°)$, and (d) $(\theta, \theta_0) = (27°, 75°)$. The optical depth τ in 2-D cases is a value averaged over all directions ($0 \leq \mu \leq 1$).

features are observed for optical depths less than 4. These include the subsun (SS) and lower sunvex Parry arc (LSVP) in the reflected intensity (these are also visible for an optical depth of 16), and the circumzenithal arc (CZA) and upper suncave (USCP) and sunvex (USVP) Parry arcs in the transmitted intensity. For 2-D columns, the lower tangent arc (LTA) is noticeable in the reflected intensity for all optical depths. The upper tangent arc (UTA) is observable in the transmitted intensity for optical depths less than 4. When the optical depth is large, the transmitted intensities have the lowest values in the zenith and nadir directions, as shown in Figs. 5 and 6. Except for these features, the reflected and transmitted intensities of 2-D columns are similar to those of randomly oriented columns. Also, it is noted that the reflected and transmitted intensity distributions of Parry columns are similar to those of 2-D columns for large optical depths ($\tau = 16$) because sufficient multiple scattering is present.

The effects of orientation on reflection are shown in Fig. 7. As shown in Fig. 7a, plates reflect more solar flux when they are horizontally oriented, as compared with random orientation in space. An exception is when the sun is nearly overhead. In this case, the forward transmission by horizontally oriented plates is most significant, thereby reducing the reflection values. The reflection patterns for Parry and 3-D columns also show large differences. For large μ_0, Parry columns reflect less solar flux because of large forward transmission. However, for small μ_0, due to a longer effective optical pathlength, the reverse is true. The reflection patterns for 2-D and 3-D columns are extremely similar, however.

Finally, we discuss the polarization pattern for ice crystal clouds computed from the present program. Figure 8 shows the linear polarization ($-Q/I$) of sunlight reflected by 3-D plates ($L/2a = 0.1$) and 3-D columns ($L/2a = 2.5$) with an overhead sun ($\theta_0 = 0°$) for optical depths of ¼, 1, 4, and 16. In this case, polarization is azimuth independent. When the optical depth is ¼, polarization deviates only slightly from that for single scattering shown in Fig. 5 of Part I. With increasing optical depth, polarization approaches zero. However, the neutral point (angle of zero polarization)

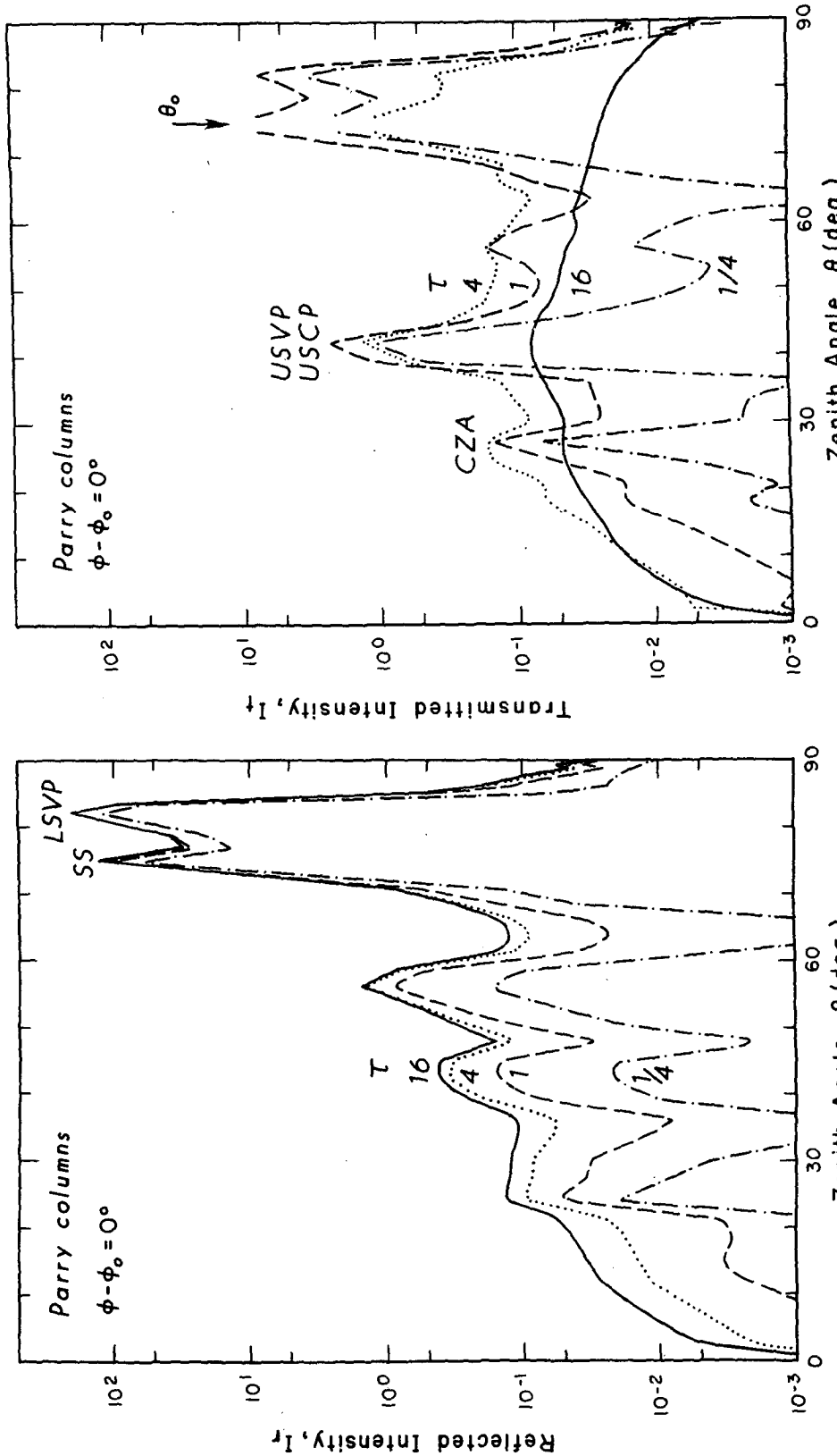

FIG. 5. Intensity of sunlight reflected and transmitted by Parry columns ($L/2a = 2.5$) in the solar principal plane ($\phi - \phi_0 = 0°$) at $\lambda = 0.55$ μm. The solar zenith angle is 75°.

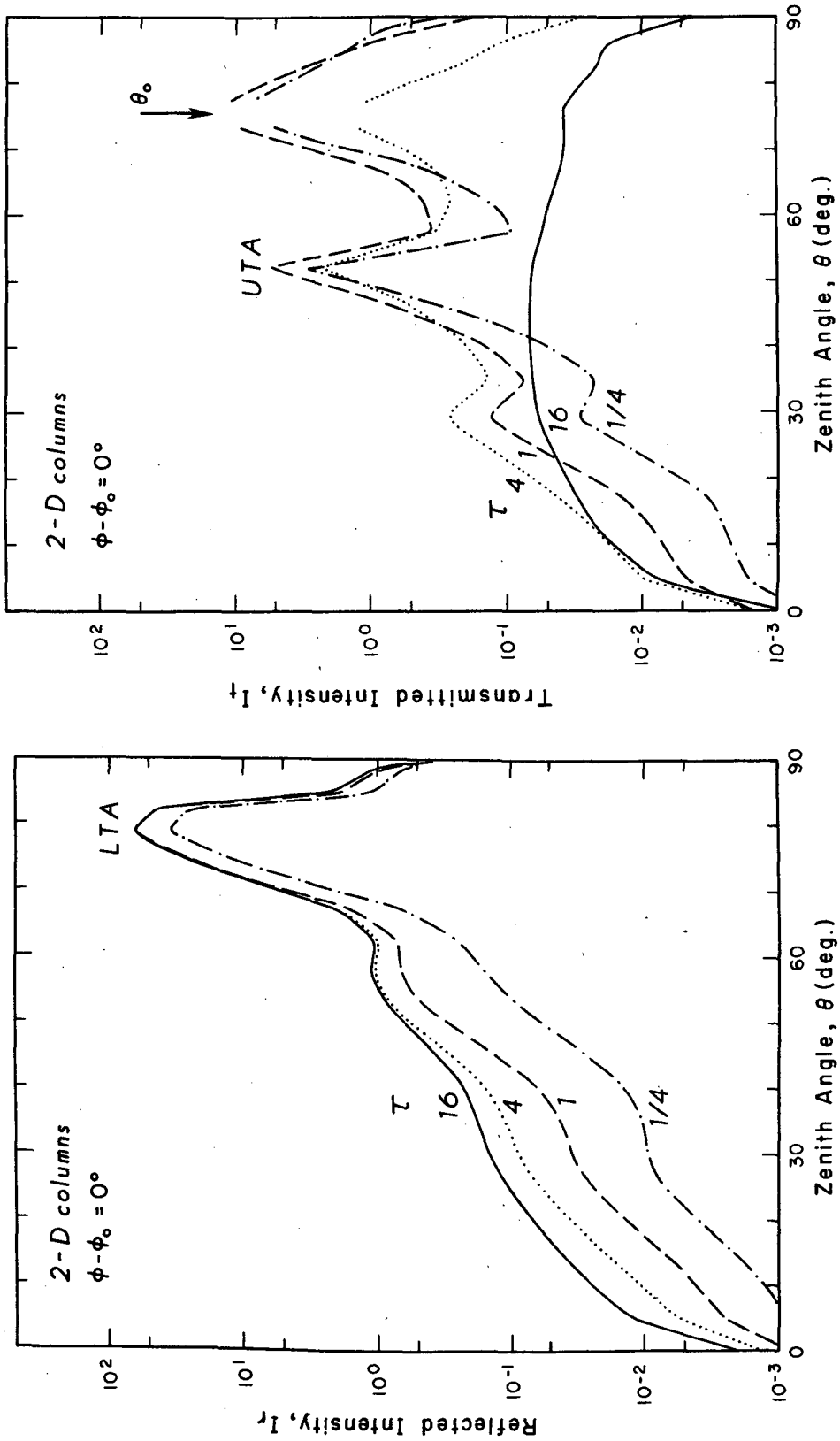

FIG. 6. As in Fig. 5, except for 2-D columns ($L/2a = 2.5$).

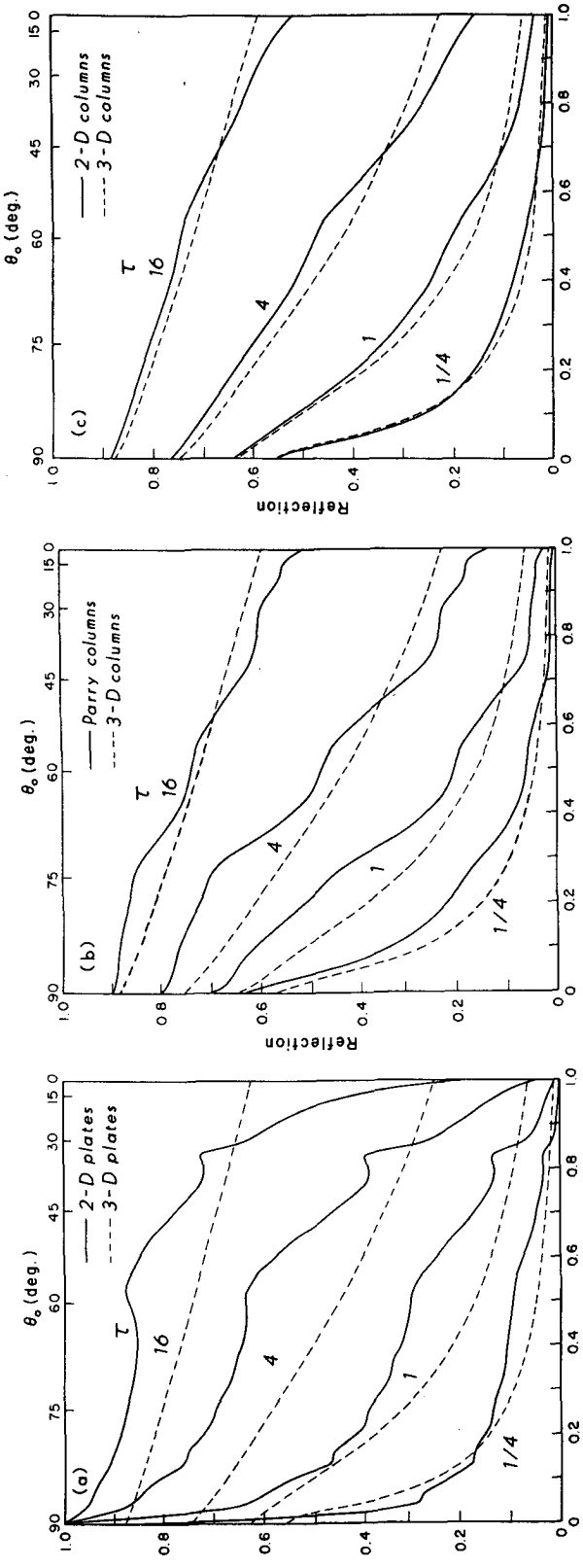

FIG. 7. Reflection (a) for 2-D and 3-D plates ($L/2a = 0.4$) as a function of the cosine of the solar zenith angle at $\lambda = 0.55$ μm, (b) for Parry and 3-D columns ($L/2a = 2.5$), and (c) for 2-D and 3-D columns ($L/2a = 2.5$).

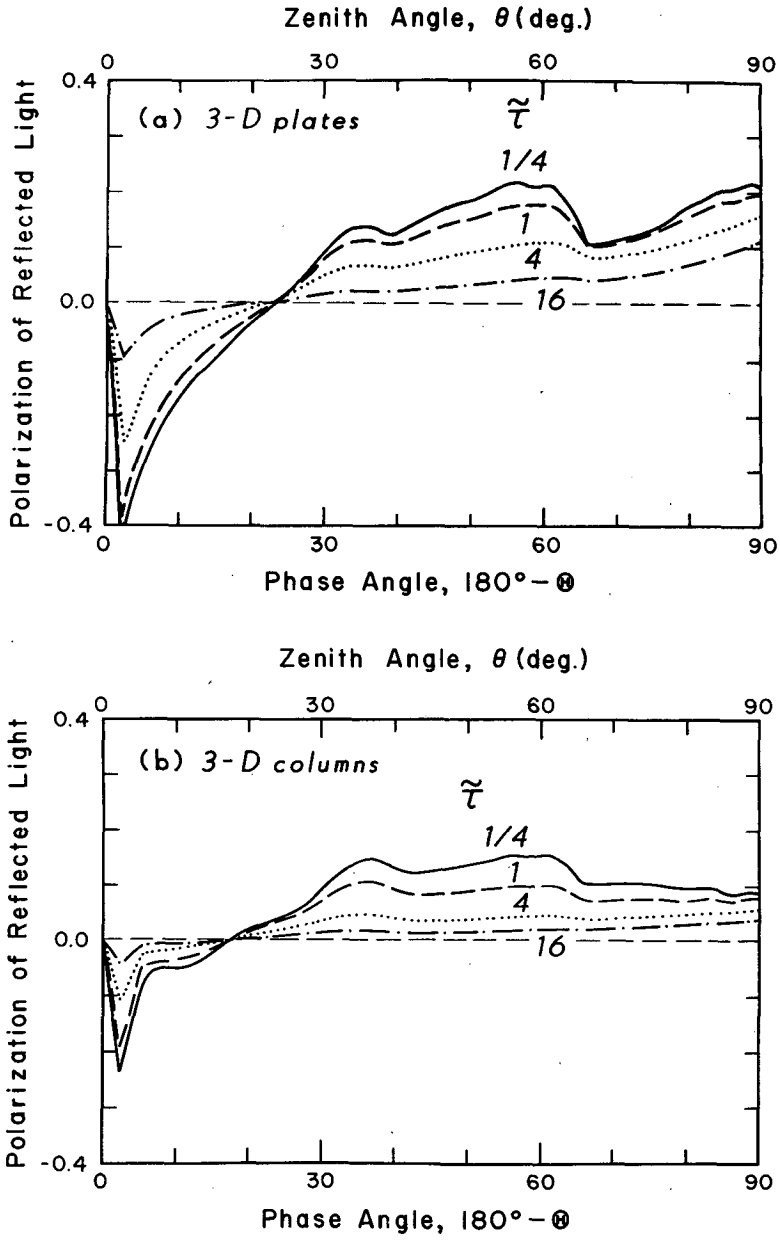

FIG. 8. Polarization, $-Q/I$ of sunlight reflected by (a) 3-D plates ($L/2a = 0.1$) and (b) 3-D columns ($L/2a = 2.5$) as a function of the phase angle, $180° - \Theta$ for an overhead sun ($\theta_0 = 0°$) at $\lambda = 0.55$ μm.

is not affected by multiple-scattering processes. This has been discussed by Hansen (1971) in the case of spherical particles.

Figure 9 shows the polarization of sunlight reflected by 3-D crystals and area-equivalent spheres in the solar principal plane ($\phi - \phi_0 = 0°/180°$) when the position of the sun is at $\theta_0 = 50°$. For ice spheres, a maximum polarization of about 80% is shown at the ~45° phase angle for an optical depth of 1 (Fig. 9a). This maximum polarization is associated with the rainbow features produced by spherical particles and is absent for ice crystal clouds. Ice plates and columns both show negative polarization maxima at phase angles close to 0°. In general, plates produce larger polarization than columns. Using an optical depth of 16, polarization decreases significantly, as shown in Fig. 9b (note that a different scale is used here). However, the polarization pattern does not vary with increasing optical depth. In particular, it is noted that the neutral points at phase angles of ~18° for columns and ~23° for plates re-

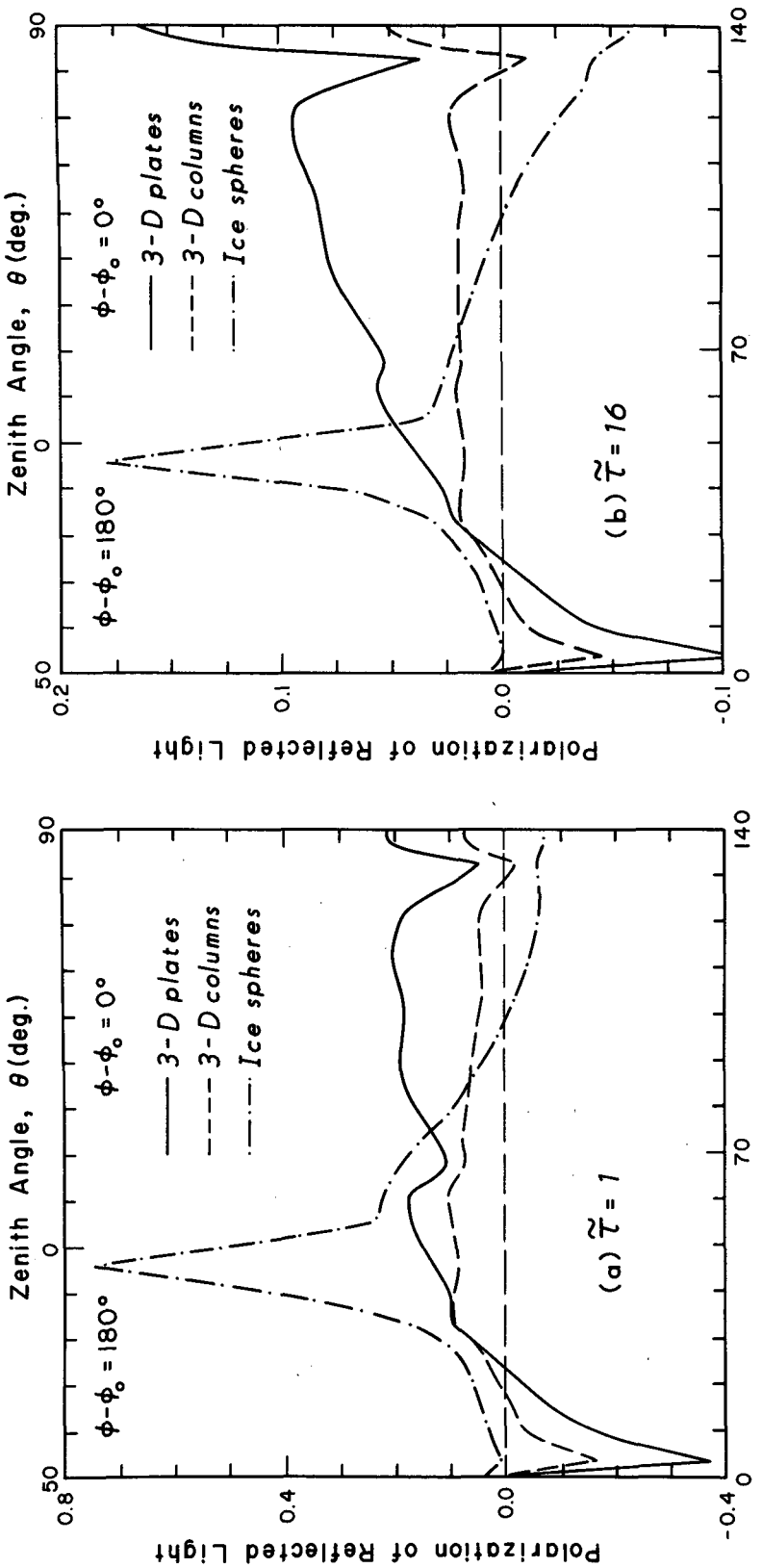

FIG. 9. Polarization of sunlight reflected by 3-D plates ($L/2a$ = 0.1), 3-D columns ($L/2a$ = 2.5), and area-equivalent spheres as a function of the phase angle in the solar principal plane ($\phi - \phi_0$ = 0°/180°) at λ = 0.55 μm. The solar zenith angle is 50°. The optical depths considered are (a) 1, and (b) 16.

main nearly constant, regardless of the optical depth. These neutral points are also independent of the incident solar angle. The preceding discussions, however, do not apply to sky polarization due to Rayleigh scattering. In the case of Rayleigh scattering, negative polarization, and hence the neutral point, are produced by double scattering (van de Hulst 1980). Thus multiple scattering, which depends on the optical depth and incident solar angle, would significantly affect the position of neutral points.

4. Interpretation of polarization measurements for ice crystal clouds

Santer et al. (1985) measured the polarization of sunlight reflected by Martian white clouds using the photopolarimeter equipment on the spacecraft MARS-5. They also presented polarization measurements using a ground-based telescope reported by Dollfus. These results are shown in Fig. 10. The two dash-dotted curves denote the fittings of polarization measured by MARS-5 at $\lambda = 0.592$ μm, assuming optical depths of ∞ and 0.3, reported by these authors. Since there is no positive peak around the 45° phase angle, the presence of water droplets is excluded. If the white clouds on Mars consist of dry ice (cubes), the neutral point should have been at ~40°, according to the computations given by Liou et al. (1983). Since this is not present in the measurements, dry ice is not a likely candidate for the particles in Martian white clouds. For interpretation purposes, randomly oriented plates and columns with an optical depth of 64 are used. As shown in Fig. 10, the neutral point of 24° for 3-D plates closely matches the observed value. It is noted that the neutral point does not vary significantly with the crystal aspect ratio (see Fig. 5a of Part I), nor with the optical depth, as illustrated in Figs. 8 and 9. The differences around the phase angle of ~5° between the observed and computed values could be explained by deviations from the exact plate- or column-like shape in the ice crystal types occurring in Martian white clouds. These differences have been noted between laboratory and model ice crystals observed by Cai and Liou (1982). On the basis of our theoretical interpretation of the neutral point, we speculate that Martian white clouds are composed of randomly oriented plate-like ice crystals.

Coffeen (1979) measured the polarization of sunlight reflected by cirrus using an infrared polarimeter aboard the NASA Convair 990. The measurement was performed on the solar principal plane, $\phi - \phi_0 = 0°/180°$ at $\lambda = 2.22$ μm. Polarization results are shown in Fig. 11. Since the observed cirrus thickness is about 5 km, we used an optical depth of 64 in the theoretical calculations. To match the observed phase angles between 0° and 160°, we used a solar zenith angle of 70°. The negative values around the 140° and 160° phase angles result from the outer and inner halos, respectively. Around the ~0° phase angles, the magnitude of negative polarization is larger than at other phase angles. This is because these directions are close to the horizon and, when the optical depth is large, multiple scattering

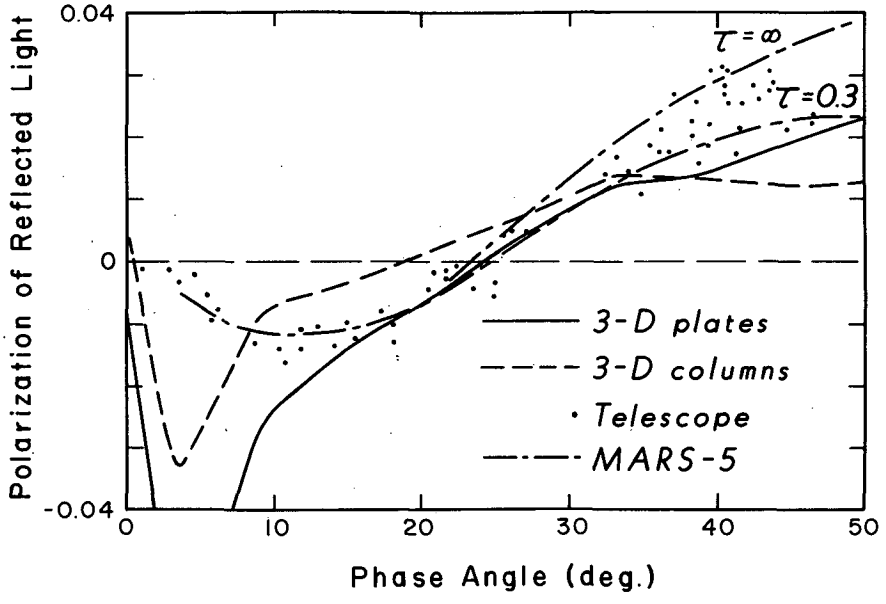

FIG. 10. Comparison of polarization of sunlight reflected by Martian white clouds between the measurements reported by Santer et al. (1985) and the present computation. The ice crystal models used for interpretation are 3-D plates ($L/2a = 0.1$) and 3-D columns ($L/2a = 2.5$) at $\lambda = 0.55$ μm with an optical depth of 64.

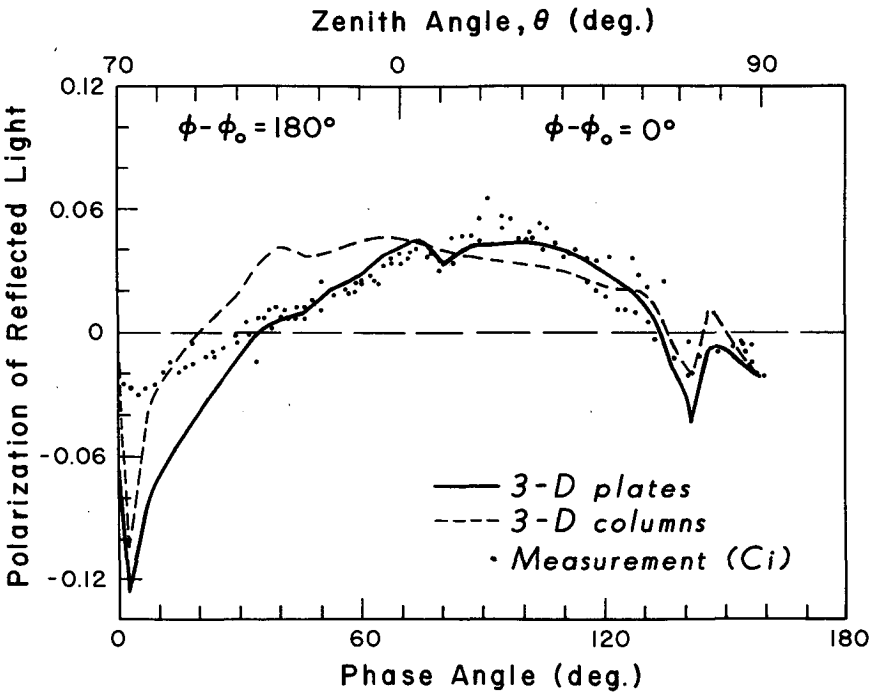

FIG. 11. Comparison of polarization of sunlight reflected by cirrus at $\lambda = 2.22$ μm between measurements reported by Coffeen (1979) and the present computation. The ice crystal models used are 3-D plates ($L/2a = 4$ μm/40 μm) and 3-D columns ($L/2a = 100$ μm/40 μm) with an optical depth of 64.

is relatively less important. Thus, polarization of the reflected sunlight is produced mostly by single scattering. Since there is no sharp peak due to the rainbow feature around the ~45° phase angle in the observed polarization, the cloud particles must be nonspherical. The computed polarization for plates fits the observed values quite well. We conclude that the cloud particles near the cloud top must be randomly oriented plate-like ice crystals. The differences between the computed and observed polarization around the 0° phase angle may be explained as follows: in backward directions, i.e., the 0° phase angle, it is possible that singly scattered light is blocked by the body of the airplane and only multiple-scattered light with small polarization can reach the polarimeter. Also, it is likely that the cloud contains irregular ice crystals, which specifically reduce polarization in the backscattering directions.

The interpretation of polarization measurements presented here, however, is meant to demonstrate the applicability of the multiple-scattering program developed for hexagonal ice crystals. For absorption wavelengths, ice crystal size distributions could be important in the determination of scattering and polarization results. This is an area requiring further research. In particular, concurrent cloud physics measurements are needed in order to develop remote sounding techniques for the detection of ice crystal clouds using the principle of multiple scattering and polarization.

5. Conclusions

In this paper, radiative transfer of polarized light in an anisotropic medium has been formulated with the aid of the adding principle. The iterative equations developed have been used to compute bidirectional intensities for randomly and horizontally oriented ice crystals. The single-scattering parameters, including the phase function, single-scattering albedo, and extinction cross section derived for ice crystals, were incorporated in the multiple-scattering computations. In addition, we have utilized the similarity principle for radiative transfer to account for the diffraction peak and δ-forward transmission due to two refractions in the multiple scattering computations.

For the reflected and transmitted intensities, we show that there are significant differences in these intensities between hexagonal ice crystals and equivalent spheres with either the same surface area or volume. A peak in the reflected intensity associated with the rainbow features of spherical particles is absent in the case of ice crystals. This leads us to conclude that the spherical model is inadequate for use in the interpretation of bidirectional reflectance from cirrus clouds. The transmitted intensity patterns for ice crystals differ distinctly from those for ice spheres, principally due to the 22° and 46° halo maxima produced by the hexagonal structure. In regard to the crystal orientation, horizon-

tally oriented plate and column crystals produce numerous optical features in the reflected and transmitted intensity patterns, which are absent if crystals are randomly oriented in space. The planetary albedo for horizontally oriented crystals is lower than that for randomly oriented crystals when the sun is near the zenith, whereas the reverse is true when the sun is close to the horizon.

With respect to the polarization of sunlight reflected by ice crystal clouds, we show that the neutral point is independent of the solar zenith angle, as well as the optical depth. The computed polarization patterns for hexagonal ice crystals reveal notable differences from those for ice spheres and other particle shapes, such as cubes. In particular, we find that the neutral point of the reflected sunlight is very sensitive to the particle shape. This suggests that a detection of the neutral point in the polarization pattern could provide a means for the identification of the particle shape.

Finally, we interpret the polarization patterns for Martian white clouds observed from the MARS-5 spacecraft in the visible wavelength and for a cirrus cloud observed from a near infrared polarimeter aboard the NASA Convair 990. We show that the computed polarization for randomly oriented ice plates can match the observed data for a large range of phase angles. This leads us to speculate that the top of these clouds is composed of randomly oriented plate-like ice crystals. In summary, there is significant information content in the polarization pattern for sunlight reflected by clouds. It appears that polarization measurements could be effectively utilized for the identification of the particle characteristics of clouds.

Acknowledgments. All the computations contained in this research were carried out on the San Diego supercomputer, CRAY X-MP/48. The research was supported in part by NASA Grant NAG5-732 and NSF Grant ATM85-13975. We thank Graeme Stephens and the other anonymous reviewer for constructive comments on the paper. Sharon Bennett typed and edited the manuscript.

REFERENCES

Asano, S., 1983: Transfer of solar radiation in optically anisotropic ice clouds. *J. Meteor. Soc. Japan,* **61,** 402–413.

Cai, Q., and K. N. Liou, 1982: Polarized light scattering by hexagonal ice crystals: Theory. *Appl. Opt.,* **21,** 3569–3580.

Chandrasekhar, S., 1960: *Radiative Transfer.* Dover, 393 pp.

Coffeen, D. L., 1979: Polarization and scattering characteristics in the atmosphere of Earth, Venus, and Jupiter. *J. Opt. Soc. Am.,* **69,** 1051–1064.

Dave, J. V., 1970: Coefficients of the Legendre and Fourier series for the scattering functions of spherical particles. *Appl. Opt.,* **9,** 1888–1896.

Hansen, J. E., 1971: Multiple scattering of polarized light in planetary atmospheres. Parts I and II. *J. Atmos. Sci.,* **28,** 120–125, 1400–1426.

Hovenier, J. W., 1969: Symmetry relationships for scattering of polarized light in a slab of randomly oriented particles. *J. Atmos. Sci.,* **26,** 488–499.

Kattawar, G. W., S. J. Hitzfelder and J. Binstock, 1973: An explicit form of the Mie phase matrix for multiple scattering calculations in the I, Q, U, and V representation. *J. Atmos. Sci.,* **30,** 289–295.

Lacis, A. A., and J. E. Hansen, 1974: A parameterization for the absorption of solar radiation in the earth's atmosphere. *J. Atmos. Sci.,* **31,** 118–133.

Liou, K. N., 1980: *An Introduction to Atmospheric Radiation.* Academic Press, 392 pp.

——, Q. Cai, J. B. Pollack and J. N. Cuzzi, 1983: Light scattering by randomly oriented cubes and parallelepipeds. *Appl. Opt.,* **22,** 3001–3008.

Peebles, G. H., and M. S. Pleeset, 1951: Transmission of gamma rays through large thicknesses of heavy materials. *Phys. Rev.,* **81,** 430–439.

Potter, J. E., 1970: The delta function approximation in radiative transfer theory. *J. Atmos. Sci.,* **27,** 945–951.

Ripley, E. A., and B. Saugier, 1971: Photometeors at Saskatoon on 3 December 1970. *Weather,* **26,** 150–157.

Santer, R., M. Deschamps, L. V. Ksanfomaliti and A. Dollfus, 1985: Photopolarimetric analysis of the Martian atmosphere by the Soviet MARS-5 orbiter. *Astron. Astrophys.,* **150,** 217–228.

Sobolev, V. V., 1975: *Light Scattering in Planetary Atmospheres.* Pergamon, 256 pp.

Stephens, G. L., 1980: Radiative transfer in a linear lattice: Application to anisotropic ice crystal clouds. *J. Atmos. Sci.,* **37,** 2095–2104.

Stokes, G. G., 1862: On the intensity of the light reflected from or transmitted through a pile of plates. *Proc. Roy. Soc. London,* **11,** 545–556.

Takano, Y., and K. N. Liou, 1988: Solar radiative transfer in cirrus clouds. Part I: Single-scattering and optical properties of hexagonal ice crystals. *J. Atmos. Sci.* **46,** 3–19.

Tränkle, E., and R. G. Greenler, 1987: Multiple-scattering effects in halo phenomena. *J. Opt. Soc. Am., A,* **4,** 591–599.

Twomey, S., H. Jacobowitz and H. B. Howell, 1966: Matrix method for multiple scattering problems. *J. Atmos. Sci.,* **23,** 289–296.

van de Hulst, H. C., 1980: *Multiple Light Scattering.* Academic Press, 739 pp.